Catalytic Core Structure of the trans-Acting HDV Ribozyme Is Subtly Influenced by Sequence Variation Outside the Core†

Melissa E. Gondert, Rebecca A. Tinsley, David Rueda,§ and Nils G. Walter*

Department of Chemistry, The University of Michigan, 930 North University, Ann Arbor, Michigan 48109-1055

Received October 17, 2005; Revised Manuscript Received March 5, 2006

ABSTRACT: The human pathogenic hepatitis delta virus (HDV) employs a unique self-cleaving catalytic RNA motif, the HDV ribozyme, during double-rolling circle replication. Fluorescence spectroscopy, circular dichroism, terbium(III) footprinting, and X-ray crystallography of precursor and product forms have revealed that a conformational change accompanies catalysis. In addition, fluorescence resonance energy transfer (FRET) has previously been used on a trans-acting HDV ribozyme to demonstrate surprisingly significant catalytic and global conformational effects of substrate analogues with varying 5′ sequences, which reside as dangling overhangs outside the catalytic core. Here, we use the fluorescent guanine analogue 2-aminopurine (AP) in nucleotide position 76, immediately downstream of the catalytically involved C75, to monitor the relative structural effects of these substrate analogues on the ribozyme's trefoil turn of the catalytic core. Steady-state and time-resolved AP fluorescence spectroscopies show that the binding of each substrate analogue induces a unique local conformation with a specific AP_{76} stacking equilibrium. Binding of the 3′ product results in a relative increase in AP fluorescence, suggesting that AP_{76} becomes more unstacked upon catalysis. These local conformational changes are kinetically concomitant with global conformational changes monitored by FRET. Finally, the rate constant of the local conformational change upon 3′ product binding is fast and independent of 3′ product concentration yet Mg^{2+} dependent. Our results demonstrate that the trefoil turn of the HDV ribozyme catalytic core is in a state of dynamic equilibrium not captured by static crystal structures and is highly sensitive to the identity of the 5′ sequence and Mg^{2+} ions.

Conformational changes are an important strategy used by enzymes to facilitate catalysis. Such conformational changes can range from small rotations to drastic secondary structure reorganizations and may occur during any phase of a reaction to lower its energy barrier. The examination of an enzyme's conformations, as it is bound to substrates and products, has long been used as a means to elucidate the catalytic cycle of an enzyme (*1*−*3*). By analyzing the differences in the precursor and product conformations, one can often come closer to discovering how an enzyme carries out catalysis. Like protein enzymes, RNA enzymes (ribozymes) are capable of using conformational change to facilitate catalysis. Evidence of such strategy has been found, for example, in the hammerhead (*4*, *5*), hairpin (*6*−*8*), and hepatitis delta virus (HDV[1]) ribozymes (*9*−*11*), representatives of the class of small endonucleolytic ribozymes. These RNAs are characterized by their small size (<200 nucleotides) and their ability to catalyze reversible self-cleavage reactions through transesterification, and they play a central role in the replication and propagation of the associated subviral genomes.

HDV affects millions of people worldwide. It is a pathogenic RNA satellite of the hepatitis B virus (HBV), which can increase the severity of hepatitis disease symptoms, including progression to liver cirrhosis (*12*). HDV exists in nature as a single-stranded 1700-nucleotide circular genome, which is high in G-C content and shows a high degree of intramolecular base pairing. HDV replicates through a double-rolling circle mechanism to form complementary genomic and antigenomic RNA concatamers, both of which undergo self-cleavage and re-ligation into circular monomers through the action of the embedded, highly homologous, ∼85 nucleotides long catalytic RNA motifs termed the genomic and antigenomic HDV ribozymes, respectively (*12*, *13*). Site-specific cleavage occurs through deprotonation of the adjacent 2′-OH group and nucleophilic attack on the scissile phosphate to form 2′,3′-cyclic phosphate and 5′-OH termini (*10*). Both cis-(self-) and trans-cleaving forms of the HDV ribozyme have been studied to probe its catalytic mechanism (*10*); in addition, the trans-acting HDV ribozyme has potential therapeutic applications in targeted RNA inactivation (*14*−*17*).

Since its discovery, the HDV ribozyme has been the subject of extensive research. Cross-linking studies and hydroxyl radical footprinting data suggested early on the existence of a compact tertiary structure with the cleavage site phosphate buried deep within the active cleft (*18*). Crystal

† This work was supported by NIH Grant GM62357 (N.G.W.), an NIH NRSA pre-doctoral fellowship (R.A.T.), and a University of Michigan Rackham Merit pre-doctoral fellowship (R.A.T.).

* To whom correspondence should be addressed. Phone: (734) 615-2060. Fax: (734) 647-4865. Email: nwalter@umich.edu.

§ Current address: Department of Chemistry, Wayne State University, 5101 Cass Avenue, Detroit, MI 48202.

[1] Abbreviations: AP, 2-aminopurine; FRET, fluorescence resonance energy transfer; HBV, hepatitis B virus; HDV, hepatitis delta virus; NMR, nuclear magnetic resonance.

10.1021/bi052116j CCC: $33.50
Published on Web 05/27/2006

structures of the cis-cleaving genomic HDV ribozyme (*19*−*21*) report, along with prior fluorescence (*11*, *22*), NMR (*23*, *24*) and biochemical data (*23*), a change in the catalytic core structure between the precursor (substrate bound) and product forms, suggesting that a conformational change accompanies catalysis. The catalytically essential C_{75} and its two adjacent nucleotides, G_{74} and G_{76}, are observed to form a trefoil turn that pushes C_{75} toward the 5′-OH leaving group while extruding G_{76} away from the ribozyme into solution (*10*, *20*). This conformation and the fact that the identity of the base in position 76 is not essential for catalysis (*22*, *25*) provide the unique opportunity to modify G_{76} to the fluorescent guanine analogue 2-aminopurine (AP). AP can be selectively excited in the presence of the natural nucleobases and is a highly sensitive probe for changes in its local environment; it is quenched when stacked with other nucleobases but fluoresces upon exposure to solvents (*26*−*30*). Consequently, an increase in fluorescence intensity signifies the formation of the trefoil turn that extrudes AP_{76} into solution while pushing C_{75} into the active site (*22*). Using steady-state and time-resolved AP fluorescence spectroscopies on a trans-acting form of the HDV ribozyme in complex with various substrates and 3′ product analogues for comparison, we are, therefore, able to examine the relative range of catalytic core conformations that the HDV ribozyme samples during its reaction cycle.

In the product crystal structure (*19*), confirmed by biochemical studies (*31*, *32*), the short helix P1.1 bolsters the cleavage site G_1·U_{39} wobble pair through stacking interactions (Figure 1), leaving little room in the active cleft for the dangling nucleotides 5′ of the cleavage site. Therefore, it was proposed that such a 5′ sequence is accommodated by the bending of the substrate (*10*, *11*). To test this idea, several groups examined the contribution of the 5′ sequence to catalysis in trans-cleaving HDV ribozymes (*9*, *33*, *34*). Variations in the N_{-1} and N_{-2} positions were found to have a strong (up to 100-fold) effect on the cleavage rate constant (e.g., $U_{-1} > C_{-1} > A_{-1} > G_{-1}$). Furthermore, the rate of cleavage was observed to be impacted by the length and composition of up to four nucleotides in the 5′ sequence (*33*). To explain these results, a ground-state destabilization model was proposed (*9*, *34*): The densely packed catalytic core cannot accommodate the dangling 5′ sequence substrate so that the substrate is bent around the cleavage site, destabilizing the ground state; the amount of destabilization depends on the identity of the N_{-1} and N_{-2} nucleotides and, to a lesser extent, substrate length. The recently solved crystal structure of the precursor form of the cis-cleaving, genomic HDV ribozyme supports this hypothesis; electron density at the active site shows that the substrate strand makes an ~180° turn about the scissile phosphate while wedging into the catalytic core and splaying apart the two major helical stacks, P1/P1/1/P4 and P2/P3 (*21*). Accordingly, fluorescence resonance energy transfer (FRET) studies were able to detect strong effects of the 5′ sequence on the global conformation of a trans-acting ribozyme (*34*), yet the effects on the conformation of the deeply embedded catalytic core remained largely unresolved.

Here, we have used our previously characterized trans-cleaving HDV ribozyme (*11*, *22*, *34*−*36*) in conjunction with a 3′ product and six substrate analogues of varying 5′ sequences to observe the relative structural effects that a

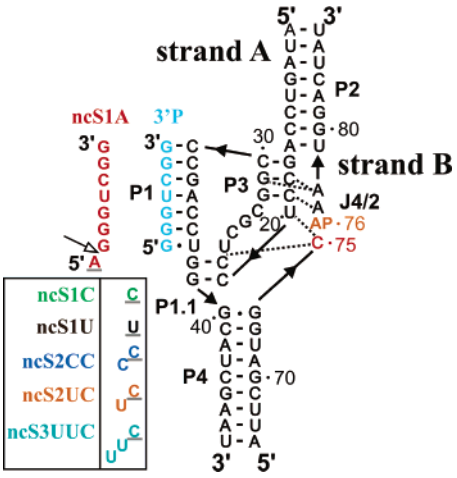

FIGURE 1: Synthetic HDV ribozyme construct D1. The ribozyme consists of two separate RNA strands A and B. Fluorescent guanine analogue 2-aminopurine (AP, orange) is incorporated at position 76 in the joiner sequence J4/2, which contains the trefoil turn motif. The catalytically involved C_{75} is shown in red. For FRET studies, donor (fluorescein) and acceptor (tetramethylrhodamine) fluorophores were coupled to the 5′ and 3′ termini of strand B, respectively, as described (*11*). The 3′ product (3′P, light blue) is shown in complex with the ribozyme. The noncleavable substrate analogue ncS1A contains one additional nucleotide 5′ of the cleavage site (arrow). Other substrate analogues with varying 5′ sequences are shown in the box. To render substrate analogues noncleavable, the 2′-OH groups of the nucleotides underlined in gray immediately 5′ of the cleavage site were modified to 2′-methoxy groups of similar sugar pucker preference. Dashed lines represent tertiary hydrogen bonds of C_{75} and the ribose zipper of A77 and A78 in joiner J4/2, flanking AP_{76}. Dashes between bases represent Watson Crick base pairs, whereas dots represent non-Watson Crick base pairs.

varying 5′ sequence has on active site conformation. We find that the binding of each substrate analogue induces a unique catalytic core conformation in which the distribution of AP_{76} between different stacking environments, as quantified by time-resolved AP fluorescence spectroscopy, differs from that in the 3′ product bound form. We correlate the local conformational changes upon cleavage of the various substrates with kinetically concomitant global conformational changes monitored by FRET. We also find that the rate constant of the local conformational change upon 3′ product binding is fast and independent of the 3′ product concentration, suggesting that in this case, not binding but conformational relaxation is rate-limiting. Our results emphasize that the trefoil turn of the HDV ribozyme catalytic core is in a state of dynamic equilibrium not captured by the static crystal structure, which is dependent on the identity of the 5′ sequence and Mg^{2+} ions and is related to distinct global architectures and catalytic activities.

MATERIALS AND METHODS

Preparation of RNA Oligonucleotides. RNA oligonucleotides (for sequences see Figure 1) were obtained commercially from the HHMI Biopolymer/Keck Foundation Biotechnology Resource Laboratory at the Yale University School of Medicine or from Dharmacon, Inc. (Lafayette, CO). The 2′-OH protection groups were removed according to the manufacturer's recommended protocol. Deprotected oligonucleotides were purified by denaturing 20% polycacrylamide, 8 M urea gel electrophoresis, diffusion elution

Table 1: Binding and Dissociation Rate Constants of the Substrate Analogues and the 3′ Product[a]

	k_{on} ($min^{-1} M^{-1}$)	k_{off} (min^{-1})
ncS1A	$(1.9 \pm 0.4) \times 10^6$	0.08 ± 0.02
ncS1C	$(1.3 \pm 0.4) \times 10^6$	0.11 ± 0.05
ncS1U	$(6.4 \pm 1.2) \times 10^5$	0.15 ± 0.06
ncS2CC	$(1.4 \pm 0.1) \times 10^6$	0.04 ± 0.02
ncS2UC	$(6.9 \pm 3.0) \times 10^5$	0.20 ± 0.06
ncS3UUC	$(1.4 \pm 0.2) \times 10^4$	0.20 ± 0.06
3′P	$\geq (8.0 \pm 1.1) \times 10^6$	n/a

[a] The binding rate constant k_{on} and the dissociation rate constant k_{off} were determined as described in Materials and Methods under standard conditions: 40 mM Tris-HCl at pH 7.5 and 11 mM $MgCl_2$ at 25 °C. The k_{on} value was obtained from the steady-state AP_{76} fluorescence data in Figure 2. The errors in k_{on} were derived from the error in slope as determined by five measurements of k_{obs} at various substrate analogue concentrations. The k_{off} value was determined from 3′P chase experiments (Materials and Methods), which were not applicable (n/a) for the 3′ product itself. The errors in k_{off} were derived from at least two independent measurements.

into 0.5 M NH_4OAc, 0.1% SDS, and 0.1 mM EDTA overnight at 4 °C, chloroform extraction, ethanol precipitation, and C_8 reverse-phase HPLC with a linear acetonitrile gradient in triethylammonium acetate, as described (*37*, *38*). Noncleavable substrate analogues were modified with a 2′-methoxy group at the cleavage site with a similar sugar pucker preference as the native 2′-OH. For FRET studies, a 5′-fluorescein was coupled to strand B during synthesis, whereas tetramethylrhodamine was postsynthetically attached to a 3′-amino linker, as previously described (*11*, *38*). RNA concentrations were calculated on the basis of their absorbance at 260 nm. When necessary, corrections were made for the additional absorbance of fluorescein and tetramethylrhodamine by using the relationships $A_{260}/A_{492} = 0.3$ and $A_{260}/A_{554} = 0.49$, respectively.

Steady-State Fluorescence Spectroscopy. Experiments were conducted under standard conditions of 40 mM Tris-HCl at pH 7.5 and 11 mM $MgCl_2$ at 25 °C, unless otherwise stated. For FRET measurements, the standard buffer was supplemented with 25 mM dithiothreitol as the oxygen scavenger. HDV ribozyme was heat-annealed from an excess of 400 nM unlabeled strand A over 200 nM labeled strand B by heating at 70 °C for 2 min, followed by cooling to room temperature for 5 min. Noncleavable substrate analogues and the 3′ product were prepared to reach final concentrations ranging from 1 to 3 μM, whereas cleavable substrates were prepared at final concentrations of 1 μM. Pre-annealed ribozyme and substrates solutions were then separately incubated for 15 min at 25 °C.

Fluorescence spectra and time traces were recorded on an Aminco-Bowman Series 2 (AB2) spectrofluorometer (Thermo Electron Corporation, Houston, TX). AP was excited at 290 nm (4 nm bandwidth), and the emission was measured at 360 nm (16 nm bandwidth). For FRET measurements, fluorescein was excited at 490 nm (4 nm bandwidth), and fluorescence emission was recorded simultaneously at the fluorescein (520 nm, 16 nm bandwidth) and tetramethylrhodamine (585 nm, 16 nm bandwidth) wavelengths. The noncleavable substrate analogue, cleavable substrate, or the 3′ product was manually added to the ribozyme-containing cuvette (3 mm path length, 150 μL volume) 60 s after starting a measurement. For analysis, emission signals were normalized to their values prior to the addition of the substrate analogue. Resulting time traces were fit in Origin 7.0 as necessary to double-exponential increase or decrease functions of the form $y = y_0 + A_1 (1\text{-}e^{t/\tau 1}) + A_2 (1\text{-}e^{t/\tau 2})$ and $y = y_0 + A_1 e^{-t/\tau 1} + A_2 e^{-t/\tau 2}$, respectively, where y_0 is the y-intercept, A is the amplitude, and $1/\tau 1$ and $1/\tau 2$ yield fast- and slow-phase rate constants, respectively. For substrate analogue ncS3UUC, a single-exponential increase function of the form $y = y_0 + A_1 (1\text{-}e^{x/\tau 1})$ was sufficient to fit the time traces. The resulting pseudo-first-order rate constants were generally linearly dependent on the excess concentration of substrate, indicating that the observed fluorescence increase is a direct result of substrate binding (*11*, *22*). Thus, fast-phase rate constants, averaged over at least two independent experiments, were plotted over the noncleavable substrate analogue or 3′ product concentration to obtain bimolecular substrate binding rate constants from the slope, as reported in Table 1. Additionally, the pseudo-first-order rate constants of 3′ product binding were plotted in dependence of magnesium concentration and fit with a modified Hill equation of the form

$$k_{obs} = A_0 + k_{max} \frac{[Mg^{2+}]^n}{[Mg^{2+}]^n + Mg_{1/2}{}^n} \quad (1)$$

where A_0 is the offset, k_{max} is the cleavage rate under saturating Mg^{2+} conditions, $Mg_{1/2}$ is the magnesium half-titration point, and n is the cooperativity constant.

To obtain substrate dissociation rate constants, a 3-fold excess (at least) of the 3′ product over substrate was added to an equilibrated ribozyme−noncleavable substrate analogue complex, as previously described (*22*). The resultant fluorescence intensity increases were fit to double-exponential increase functions, and the fast-phase substrate dissociation rate constants (k_{off}) are reported in Table 1. Errors represent the standard deviation as determined by two or more repeat measurements.

Time-Resolved Fluorescence Spectroscopy. The local environment of AP_{76} was probed under standard conditions using time-resolved fluorescence spectroscopy as described (*39*, *40*). Specifically, the ribozyme−noncleavable substrate analogue complex or the ribozyme−product complex (75 μL; 1 μM ribozyme strand B, 3 μM strand A, and 6 μM substrate, noncleavable substrate analogue, or 3′ product; for the two-strand construct J1/2-PEX-1 strand B and the long substrate strand were at 1 μM and 3 μM, respectively) was heat-annealed and incubated in standard buffer at 25 °C (for J1/2-PEX-1 and 3S-PEX-1, the conditions were 25 mM acetic acid, 25 mM MES, 50 mM Tris-HCl (pH 7.5), and 11 mM $MgCl_2$ at 37 °C) for at least 15 min. Time-resolved emission profiles were then collected using time-correlated single-photon counting: a frequency-doubled Nd:YVO4 laser (Spectra-Physics Millenia Xs-P, operated between 8 and 8.5 W) pumped a frequency-doubled, mode-locked Ti:sapphire laser (Spectra-Physics; operated at 1 W) to excite AP at 347 nm with pulses 2 ps in width, picked down to 4 MHz. Isotropic emission to >20 000 peak counts was detected under magic angle polarizer conditions at 360 nm (10-nm band-pass interference filter). An instrument response function was measured as the scattering signal from a dilute solution of nondairy coffee creamer to deconvolute the fluorescence decay data. The obtained emission decays were

Table 2: Fluorescence Intensity Decay Times of Various Ribozyme−Substrate Analogue and Ribozyme−Product Complexes[a]

	$\tau 1$	$\tau 2$	$\tau 3$	$\tau 4$
ncS1A	0.113 (75%)	0.93 (15%)	3.76 (6%)	10.2 (4%)
ncS1C	0.073 (83%)	0.78 (10%)	3.29 (5%)	9.11 (2%)
ncS1U	0.076 (84%)	0.72 (9%)	2.88 (4%)	8.78 (3%)
ncS2CC	0.098 (81%)	0.83 (11%)	3.06 (6%)	8.11 (2%)
ncS2UC	0.077 (81%)	0.78 (11%)	3.10 (6%)	8.33 (2%)
ncS3UUC	0.082 (78%)	0.64 (13%)	2.51 (7%)	7.79 (2%)
3′P	0.054 (77%)	0.69 (13%)	3.04 (4%)	9.46 (6%)
3S-PEX-1-ncS	0.020 (91%)	0.61 (5%)	2.62 (3%)	7.63 (1%)
3S-PEX-1-3′P	0.048 (94%)	0.70 (2%)	2.90 (1%)	9.10 (2%)
J1/2-PEX-1-ncS	0.027 (87%)	0.58 (7%)	2.86 (4%)	8.36 (2%)
J1/2-PEX-1-3′P	0.027 (88%)	0.74 (6%)	3.71 (3%)	9.48 (3%)

[a] Fluorescence decay time constants were determined as described in Materials and Methods under standard conditions: 40 mM Tris-HCl at pH 7.5 and 11 mM $MgCl_2$ at 25 °C.

fit with multiexponential decay functions as described above to each yield four decay time constants τ_i and amplitudes A_i, as reported in Table 2 (*39*, *40*).

RESULTS

Catalytic Core Conformation of the HDV Ribozyme Depends on Dangling Nucleotides 5′ of the Cleavage Site. The trans-cleaving HDV ribozyme construct D1 utilized in this study consists of three strands; ribozyme strands A and B and a substrate analogue or product strand (Figure 1). The catalytic activity of this ribozyme has previously been characterized under a variety of conditions and was shown to be at least equal to that of other trans-acting HDV ribozymes (*11*). In addition, we have used FRET to characterize global conformational changes induced by the binding of substrate analogues with different 5′ sequences; a slight to significant decrease in FRET was observed for each analogue, indicating conformational extension of the RNA between the fluorophore attachment sites at the P2 and P4 termini (*34*). To observe localized structural changes in the catalytic core of the ribozyme, we modified G_{76} of the HDV ribozyme to the fluorescent 2-aminopurine (AP). AP is a fluorescent base that is highly sensitive to local stacking interactions with other bases (excitation at 320 nm, emission maximum at 360 nm, 68% quantum yield). When AP stacks with neighboring bases, its fluorescence becomes quenched; consequently, when AP is fully exposed to solvents its fluorescence increases substantially (*29*, *41*, *42*). Upon monitoring conformational changes around position 76 in our wild-type trans-acting ribozyme by AP_{76} fluorescence, we observed a substantial local conformational change that accompanied catalysis. This local conformational change was found to occur simultaneously with global conformational changes as observed by FRET (*22*). This was confirmed by terbium(III)-mediated footprinting, which showed that there are detectable and widespread structural differences between precursor (substrate bound) and product forms of the trans-acting HDV ribozyme as is the case between the precursor and the product of the cis-acting antigenomic ribozyme (*43*) and that these differences are modulated in response to the identity and length of the 5′ sequence (*34*). We therefore set out to examine the impact of the 5′ substrate sequence on the catalytic core conformation of our trans-acting HDV ribozyme by monitoring and comparing the AP_{76} fluorescence upon binding and dissociation of each of the various substrate analogues with that of the 3′-product complex (Figure 1).

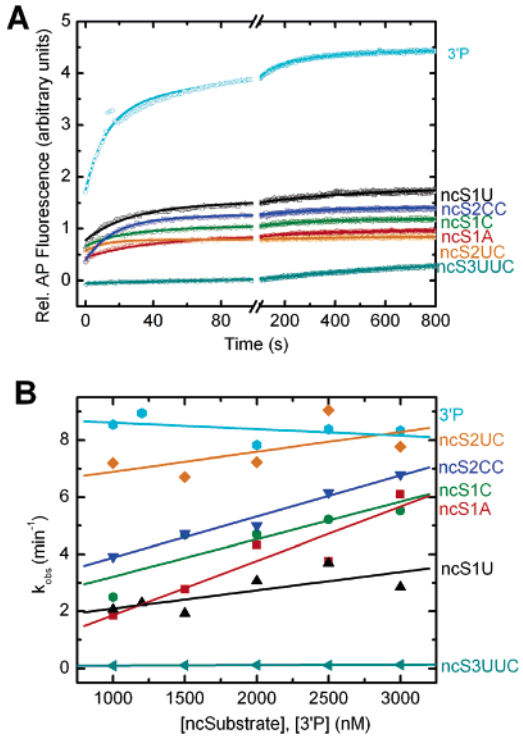

FIGURE 2: AP Fluorescence detection of substrate analogue binding in 40 mM Tris-HCl (pH 7.5) and 11 mM $MgCl_2$ at 25 °C (color-coded as in Figure 1). (A) Fluorescence time traces upon the addition of a 5-fold excess of substrate analogue over HDV ribozyme. Data were fit with double- or single-exponential (ncS3UUC) increase functions (Materials and Methods), yielding fast-phase, pseudo-first-order rate constants k_{obs}. (B) Plot of averaged pseudo-first-order rate constants k_{obs} for each substrate analogue over the excess noncleavable substrate analogue (or 3′ product) concentration at which they were obtained. These dependencies were fit with linear regression lines to obtain the bimolecular binding rate constants (k_{on}) as the slope (reported in Table 1).

The fluorescence changes observed for AP_{76} indicate that the 5′ substrate sequence indeed has an impact on the conformation of the catalytic core. Figure 2A shows that the addition of a saturating 5-fold (1000 nM) excess of each noncleavable substrate analogue to the AP_{76} modified ribozyme in a standard buffer (40 mM Tris-HCl, pH 7.5 at 11 mM $MgCl_2$; see Materials and Methods) at 25 °C leads to fluorescence changes of distinct extents and rates. The binding of all noncleavable substrate analogues (ncS..., Figures 1 and 2) to the ribozyme results in a slight to significant increase in relative AP_{76} fluorescence but not to the same extent or at the same fast rate as the binding of the 3′ product (3′P), which lacks the 5′ substrate sequence. By fitting our steady-state fluorescence time traces with double-exponential increase functions (single-exponential for ncS3UUC), we extracted a fast-phase rate constant that characterizes the pseudo-first-order reaction of formation of the ribozyme−noncleavable substrate analogue complex (Figure 2B). The bimolecular substrate binding rate constants k_{on} for all substrates were then extracted, as described previously (*11*, *34*, *43*), from the substrate analogue and product concentration dependencies (in the range of 1000−3000 nM) of these pseudo-first-order rate constants; the results are reported in Table 1. Interestingly, the binding of

3′P is the fastest and independent of concentration. This suggests that for the rapidly binding 3′ product conformational relaxation around AP_{76} and not binding is the rate-limiting step. Please note that none of the slow-phase rate constants exhibited a dependence on substrate analogue or product concentration (data not shown), indicating that the associated minor AP_{76} fluorescence changes occur after complex formation. Finally, as observed previously by FRET analysis, ncS3UUC binds considerably more slowly than all other substrate analogues, possibly because of the competition with the formation of helix P1.1 (Figure 1) (*34*).

Next, to assess substrate dissociation, we utilized the fact that the 3′ product has a higher affinity for binding to the HDV ribozyme than any substrate (*9*, *11*, *22*, *34*, *35*). An excess of 3′P (3 μM) was added as the chase to the preformed ribozyme−noncleavable substrate analogue complex in standard buffer at 25 °C (Materials and Methods). This resulted in an increase in AP_{76} fluorescence due to the dissociation of the substrate analogue and the replacement with 3′P. The extracted single-exponential rate constants k_{off}, which we have previously shown to be independent of the thus saturated 3′P concentration (*11*, *22*), are summarized in Table 1. Importantly, the dissociation rate constants measured by AP_{76} fluorescence are similar to those previously measured using FRET (*34*); generally, and as expected, the substrates that have the ability to additionally bind to the GG sequence of the 3′ segment of the P1.1 stem, such as S1C and S2CC, have considerably slower dissociation rate constants. However, again as previously observed via FRET, the ncS3UUC substrate analogue is the exception to this rule because its dissociation rate constant (0.205 min^{-1}) groups it with the faster dissociating substrates.

Cleavage Activity Monitored by Steady-State AP_{76} Fluorescence Detects the Formation of the Product Structure After Substrate Binding and Release of the 5′ Sequence. Previously, we have shown by steady-state fluorescence that the addition of a 5′ extended cleavable substrate called S3 to the ribozyme leads to a large increase in AP_{76} fluorescence, suggesting the rapid dissociation of the 5′ sequence and the formation of the ribozyme−3′-product complex upon cleavage. This observation is in contrast to the slight decrease in AP fluorescence resulting from the binding of the corresponding noncleavable substrate ncS3, which indicates that AP_{76} is significantly more stacked in the precursor than in the product complex (*22*). Unlike ncS3, however, we find here that the binding of all shorter noncleavable substrate analogues leads to increases in AP_{76} fluorescence, although not to the same extent or rate as in the binding of the 3′ product (Figure 2). To confirm this observation, we tested whether the increases in AP_{76} fluorescence observed upon the binding of our noncleavable substrate analogues are enhanced for the cleavable substrate versions. Indeed, the addition of saturating concentrations of the cleavable substrates (1000 nM) to the assembled ribozyme in standard buffer at 25 °C results in varying increases in relative AP_{76} fluorescence that in all cases surpass in extent to those observed upon the binding of the noncleavable substrate form (Figure 3). This enhanced fluorescence dequenching further supports the notion that AP_{76} becomes more unstacked upon cleavage of bound substrate and release of the 5′ sequence. It should be noted that the good agreement between the initial AP_{76} fluorescence rise upon the addition of cleavable and noncleavable substrates (analogues) supports our implicit assumption that the 2′-*O*-methyl modification at the cleavage site of the noncleavable analogues mimics the behavior of the native 2′-OH group.

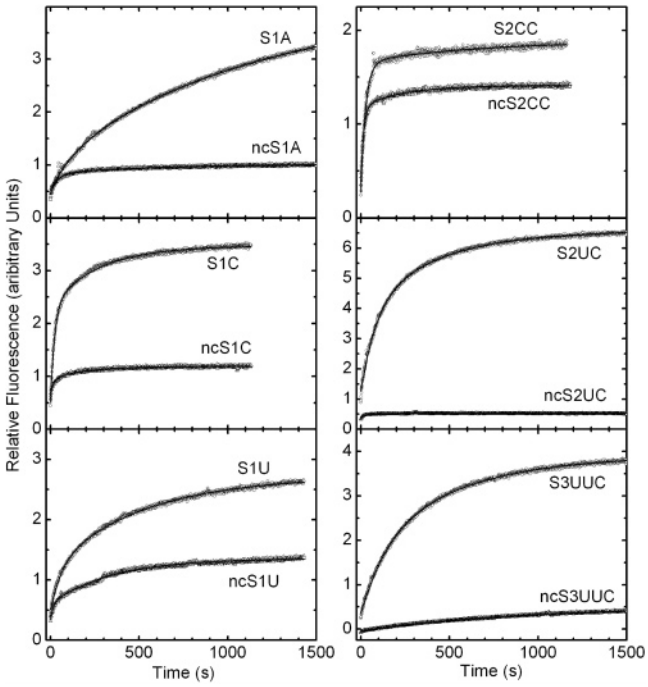

FIGURE 3: Relative steady-state fluorescence changes upon the addition of our noncleavable substrate analogues (ncS..., △, 1000 nM each) and cleavable substrates (S..., ○, 1000 nM each), respectively, to 200 nM AP_{76}-labeled HDV ribozyme D1 in 40 mM Tris-HCl (pH 7.5) and 11 mM $MgCl_2$ at 25 °C. Data were fit with double-exponential increase functions, yielding the following fast-phase rate constants for noncleavable substrate analogues and cleavable substrates, respectively: 1.855 and 0.39 min^{-1} for (nc)S1A, 2.5 and 2.86 min^{-1} for (nc)S1C, 2.07 and 0.32 min^{-1} for (nc)S1U, 3.91 and 2.05 min^{-1} for (nc)S2CC, 7.20 and 0.5 min^{-1} for (nc)S2UC, and 0.095 and 0.028 min^{-1} for (nc)S3UUC.

*Rate and Extent of AP_{76} Unstacking upon 3′ Product Binding are Dependent on Magnesium Concentratio*n. Metal ion interactions, particularly with Mg^{2+}, are crucial to the efficient folding and function of the HDV ribozyme. For example, we have previously shown that the global conformational change of the HDV ribozyme detected by FRET between a donor−acceptor pair located at the P2 and P4 termini is dependent upon Mg^{2+} concentration (*35*). We therefore set out to examine whether the local conformational change observed by AP_{76} fluorescence upon 3′P binding is also dependent on Mg^{2+} concentration. To this end, a saturating concentration (1200 nM) of 3′P was added to the assembled ribozyme in 40 mM Tris-HCl (pH 7.5) at 25 °C as a function of Mg^{2+} concentration (Materials and Methods). This resulted in a slightly double-exponential increase in AP fluorescence in which the major fast-phase rate constant was dependent on Mg^{2+} concentration. These rate constants k_{obs}, which describe the velocity of 3′P binding, were plotted as a function of Mg^{2+}, yielding an apparent Mg^{2+} half-titration point of $Mg_{1/2} = 2.6 \pm 0.6$ mM (cooperativity constant $n =$ 1.6), when fit with the modified Hill eq 1 (Figure 4A).

To also examine the relationship between the extent of AP_{76} stacking and magnesium concentration, we performed a titration in which increasing concentrations of Mg^{2+} were added to the pre-annealed ribozyme-3′ product complex in

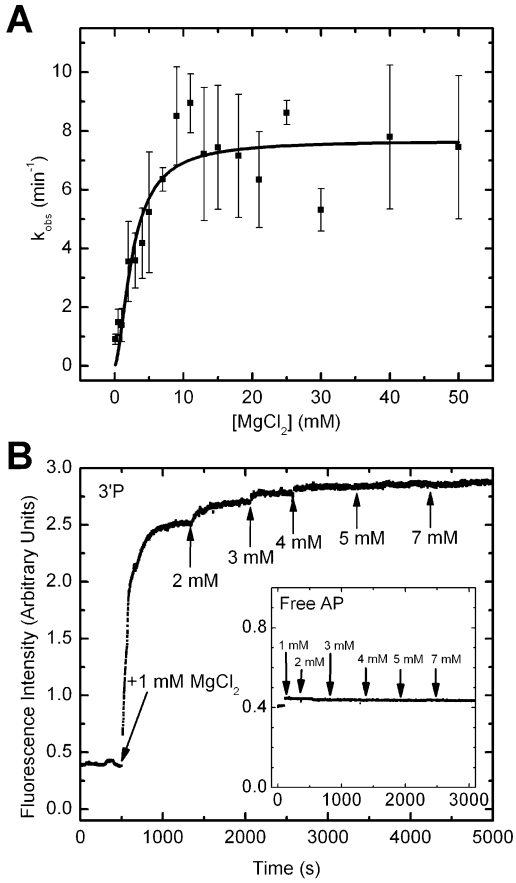

FIGURE 4: Magnesium dependence of trefoil turn folding in the ribozyme-3′ product complex under standard conditions (40 mM Tris-HCl at pH 7.5, 25 °C). (A) Dependence of the AP_{76} monitored rate constant of 3′ product binding to HDV ribozyme D1 on magnesium concentration. The 3′ product was added to the ribozyme at $MgCl_2$ concentrations ranging from 0.1 to 50 mM. Each resultant fluorescence time trace was fitted with a double-exponential increase function (Materials and Methods) to obtain the fast-phase, pseudo-first-order rate constant k_{obs}. The k_{obs} values from at least three independent experiments were averaged to obtain the data points reported here (error bars refer to standard deviations). The resultant Mg^{2+} dependence was fitted with a modified Hill equation (Material and Methods), yielding a magnesium half-titration point ($Mg_{1/2}$) of 2.6 ± 0.6 mM (cooperativity constant n = 1.6). The maximum rate constant at saturating Mg^{2+} concentration (k_{max}) is 7.7 ± 0.6 min^{-1}. (B) Dependence of the AP_{76} fluorescence on magnesium concentration, as observed by the titration of the ribozyme−3′ product complex starting at 0 mM Mg_{2+}. After 500 s of equilibration, $MgCl_2$ was added to a final concentration of 1 mM. After the fluorescence intensity had leveled off, at ~1500 s, $MgCl_2$ was again added to a final concentration of 2 mM and so forth, as indicated. The inset graph shows the identical experiment repeated with mononucleotide 2-aminopurine 2′deoxyribose 5′-triphosphate instead of the ribozyme.

40 mM Tris-HCl (pH 7.5) at 25 °C. Between 0 and 7 mM Mg^{2+}, the fluorescence intensity of AP_{76} increased 9-fold, with the largest change occurring upon the addition of just 1 mM Mg^{2+} (Figure 4B). As a control, we verified that the fluorescence of the mononucleotide 2-aminopurine 2′deoxyribose 5′-triphosphate is not Mg^{2+} dependent, that is, metal ions have no direct impact on AP fluorescence in the absence of an embedding RNA structure (Figure 4B, inset). These results suggest that both the rate and extent of conformational relaxation of AP_{76} upon 3′ product binding to our trans-acting HDV ribozyme are Mg^{2+}-dependent.

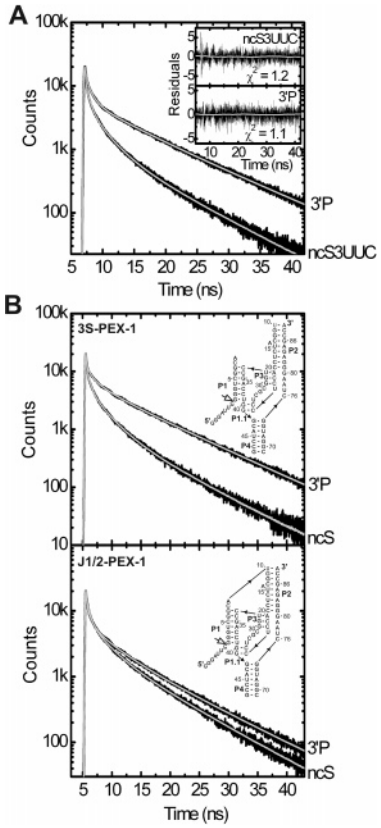

FIGURE 5: Time-resolved fluorescence decay of the precursor and product forms of several trans-acting HDV ribozyme constructs. (A) AP fluorescence decay curves of the ribozyme−ncS3UUC and ribozyme−3′ product complexes of the D1 construct in 40 mM Tris-HCl at pH 7.5 and 11 mM $MgCl_2$ at 25 °C with their corresponding exponential decay fits (grey lines). The insets show the fit residuals. (B) AP fluorescence decay curves of the precursor and product structures of the 3S-PEX-1 (top panel) and J1/2-PEX-1 (bottom panel) HDV ribozyme constructs in 11 mM $MgCl_2$, 25 mM acetic acid, 25 mM MES, and 50 mM Tris-HCl (pH 7.5) at 37 °C with their corresponding exponential decay fits. The insets show the secondary structures of the constructs.

AP_{76} Fluorescence Lifetimes Confirm that Variations in Catalytic Core Conformation Depend on 5′ Sequence Identity. Time-resolved AP fluorescence spectroscopy is a technique that resolves fast base motion and equilibria in RNA, which occur on the pico- to nanosecond time scale (*39*). Previously, it has been shown that AP that is incorporated into a nucleic acid chain exhibits four distinct lifetimes that report on different base stacking environments (*39*, *40*, *44*, *45*). The longest lifetime is typically around 10 ns and represents a completely unstacked AP, and the shortest lifetime is around 50−90 ps and represents a strongly stacked AP. The two intermediate lifetimes represent bases in the population with partial stacking interactions. To quantify the local stacking interactions of AP in our trans-acting AP_{76} HDV ribozyme, we used ps time-resolved AP fluorescence to measure emission decays for each noncleavable substrate analogue and the 3′ product in standard buffer at 25 °C. As expected, we observe a substantial difference in the fluorescence decays between the precursor and product complexes, as exemplified in the decay curves of the ribozyme−ncS3UUC and ribozyme−3′ product complexes in Figure 5A. The ribozyme−ncS3UUC complex decays faster, suggesting a decreased population of stacked AP bases compared

to that in the ribozyme−3′ product complex. Using previously described analysis procedures (Materials and Methods) (*39*, *40*), we were able to obtain four lifetimes with corresponding amplitudes for each ribozyme−noncleavable substrate complex as well as the ribozyme−3′ product complex, all reported in Table 2. Interestingly, we observed only relatively modest differences in the relative amplitudes of lifetimes between the complexes. For all substrate analogue complexes, the shortest lifetime contributes the largest amplitude (75−85%), whereas the longest lifetime represents the smallest amplitude (2−4%). In contrast, the longest lifetime, which represents a completely unstacked (solvent exposed) AP_{76}, contributes approximately 6% to the fluorescence decay of the 3′ product complex, 2- to 3-fold higher than that for the precursor complexes (Table 2). These time-resolved data support the notion that the steady-state fluorescence intensity increase upon cleavage and formation of the 3′ product complex is due to partial AP_{76} unstacking.

To verify that these differences in extent of AP_{76} stacking between the precursor and product conformations are general, we employed two other trans-acting HDV ribozymes, 3S-PEX-1 and J1/2-PEX-2 (Figure 5B, secondary structures shown as insets). These constructs are derived from the cis-acting antigenomic HDV ribozyme used in previous studies by Been and co-workers (*46*) as well as in our own studies (*43*). In construct 3S-PEX-1, both the helical crossover J1/2 and the loop L4 have been removed from the cis-acting form to create a three-strand version, similar to our D1 construct. J1/2-PEX-1 is a two-strand construct in which only the loop L4 is severed. Both constructs were modified to include a $U_{77}AP$ mutation, the antigenomic equivalent to the $G_{76}AP$ mutation used in our studies of the D1 construct. We acquired time-resolved AP fluorescence decay curves, as described above, for the precursor (ncS) and product (3′P) complexes of both constructs in a buffer containing 25 mM acetic acid, 25 mM MES, 50 mM Tris-HCl (pH 7.5), and 11 mM $MgCl_2$ at 37 °C. The two AP fluorescence decay curves for 3S-PEX-1 look very similar to those for the D1 construct; the precursor fluorescence decays significantly faster than the product fluorescence. In comparison, for the J1/2-PEX-1 construct, we observe only a slight difference between the precursor and product complexes, yet the precursor fluorescence still decays faster than the product fluorescence. These data show that there is indeed a consistent difference in the stacking interactions of AP_{76} in the catalytic core that favors unstacking in the product over the precursor conformation. In addition, there are quantitative but not qualitative differences between constructs that share the same secondary structure but differ in the connectivities of their helices.

Complementary Kinetic Studies by Steady-State FRET and AP_{76} Fluorescence on a Triply labeled Ribozyme Demonstrate the Synchronicity of Local and Global Conformational Changes. Previously, we have shown using AP fluorescence and FRET in concert that local conformational changes in the trefoil turn of the catalytic core of the HDV ribozyme kinetically coincide with global structural changes upon binding and cleavage of a specific substrate termed S3 (*22*). However, it remained to be tested whether this is a general phenomenon for conformational changes of different amplitudes and rate constants as observed upon the binding of a set of substrate analogues such as those utilized in this study. To this end, we utilized AP_{76} fluorescence and FRET in concert by employing a modified strand B of our D1 construct with the $G_{76}AP$ substitution and terminal 5′ fluorescein and 3′ tetramethylrhodamine labels as the donor−acceptor FRET pair. To ensure that this triply labeled strand (at a concentration of 200 nM) is completely converted into the substrate analogue (3′ product) complex, we added 2- and 5-fold excesses of the unmodified strand A and substrate analogue (3′ product), respectively (Materials and Methods).

Figure 6 shows the changes in relative AP_{76} fluorescence and FRET efficiency upon the addition of a 1000 nM excess of our various noncleavable substrate analogues or the 3′ product to the assembled triply labeled ribozyme in standard buffer at 25 °C. Indeed, an increase in the relative AP fluorescence and a synchronous decrease in relative FRET efficiency are observed. The resultant biphasic rate constants, listed in the Figure legend, are in reasonable agreement with the values obtained from AP_{76} probing in the absence of FRET fluorophores. These results demonstrate that the local conformational change observed through AP_{76} fluorescence upon the binding of substrate analogue or 3′ product occurs, in all cases, simultaneously with the global conformational change detected by FRET.

DISCUSSION

In recent years, the universal role of RNA in almost every aspect of cellular function has become increasingly apparent. RNA is essential to the maintenance, transfer, processing, and regulation of genetic information in the form of an endogenous messenger and noncoding RNAs as well as exogenous viral RNAs (*47*, *48*). In fact, the number of noncoding RNA genes probably far exceeds the number of protein-coding genes (*49*). Unlike proteins with their 20 or more amino acid side chains, RNA has a limited repertoire of building blocks and must, therefore, rely on its innate structural variability to facilitate its broad range of functions. A well-defined example is our trans-acting HDV ribozyme, which undergoes a change in the local environment of AP_{76} upon the binding of a substrate analogue nearly 20 Å away (Figure 7). Although nucleotides 5′ of the cleavage site are not predicted to directly base pair with the downstream sequence, one may still expect subtler effects on the ribozyme's tertiary structure. Indeed, studies have shown that the substrate binding affinity and catalytic activity of the HDV ribozyme are strongly influenced by the 5′ sequence (*9*, *33*, *34*). Studies on the energetic contribution of the 5′ sequence (*9*) and the crystal structure of the precursor ribozyme (*21*) suggest that the 5′ sequence influences affinity and activity by ground-state destabilization, where a bend in the substrate redirects substrate binding energy to lower the energetic barrier of catalysis. To further examine the structural effects of the 5′ sequence, we have previously utilized steady-state and time-resolved FRET in combination with a systematic set of noncleavable substrate analogues to demonstrate a significant correlation between the 5′ sequence and the global conformation (*34*). Here, we extend our previous work to demonstrate the effect of these 5′ sequences on the local conformation of the catalytic core, as monitored by the steady-state and time-resolved fluorescence of a 2-aminopurine, AP_{76}, embedded in the trefoil turn that also contains the catalytic C_{75}.

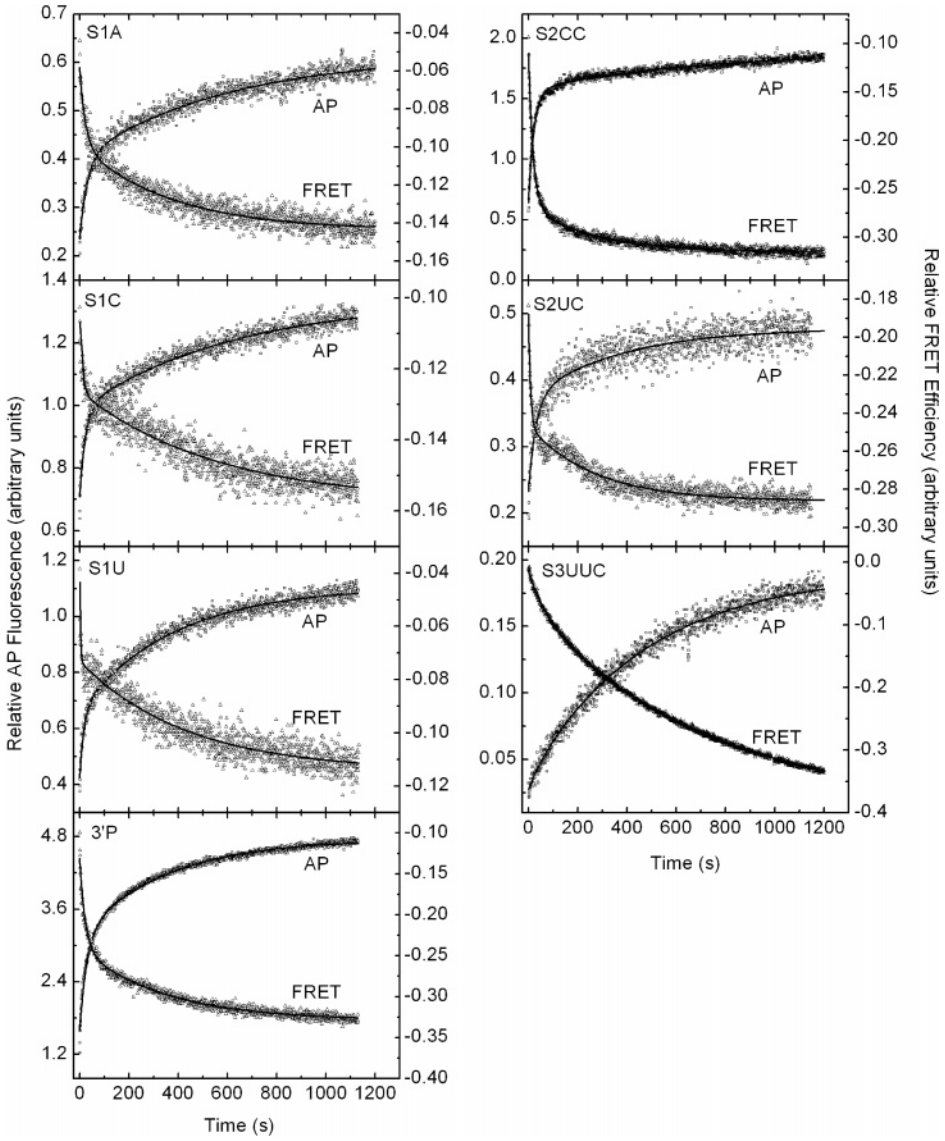

FIGURE 6: Time traces of relative AP_{76} fluorescence and relative FRET efficiency as measured on a triply (fluorescein-, tetramethylrhodamine-, and AP_{76}-) labeled ribozyme upon the addition of a 5-fold excess of substrate analogue or 3′ product. Each panel shows the AP_{76} fluorescence and corresponding steady-state FRET time traces, obtained in 40 mM Tris-HCl at pH 7.5 and 11 mM $MgCl_2$ at 25 °C. In each case, the relative AP fluorescence increase is concurrent with the relative FRET efficiency decrease. Each data set was fitted with a double-exponential increase or decrease function to obtain the following fast-phase rate constants: ncS1A, $k_{AP} = 1.8\ min^{-1}$, $k_{FRET} = 1.9\ min^{-1}$; ncS1C, $k_{AP} = 2.0\ min^{-1}$, $k_{FRET} = 6.3\ min^{-1}$; ncS1U, $k_{AP} = 2.4\ min^{-1}$, $k_{FRET} = 2.49\ min^{-1}$; ncS2CC, $k_{AP} = 2.62\ min^{-1}$, $k_{FRET} = 3.30\ min^{-1}$; ncS2UC, $k_{AP} = 5.46\ min^{-1}$, $k_{FRET} = 5.55\ min^{-1}$; ncS3UUC, $k_{AP} = 0.11\ min^{-1}$, $k_{FRET} = 0.10\ min^{-1}$; and 3′P, $k_{AP} = 7.58\ min^{-1}$, $k_{FRET} = 3.43\ min^{-1}$.

Variations in 5′ Substrate Sequence Impact Catalytic Core Structure, Translating into Distinct Local and Global Conformations and Catalytic Activities. AP has been previously used to monitor local conformational changes in the hammerhead (*50*, *51*) and hairpin ribozymes (*40*, *52*) as well as in aptamer (*53*, *54*), kissing loop (*55*), tetraloop (*56*), and HIV RRE RNAs (*57*). When AP is stacked with natural nucleobases, its fluorescence is quenched, whereas when solvent exposed, it fluoresces (is dequenched) (*42*). Although a structural interpretation of fluorescence spectroscopy data is generally challenging, relative comparisons of AP stacking preferences among different reaction states and RNA constructs are a powerful approach to zooming in on local structural rearrangements in the critical regions of an RNA. Previous studies on the HDV ribozyme, for example, have found that upon cleavage of a specific substrate a significant increase in AP_{76} fluorescence was observed (*22*), consistent with the idea that the nucleotide in position 76 unstacks from its neighbors in the trefoil turn as is observed in the product crystal structure (*19*). Here, we find that both steady-state and time-resolved AP fluorescence are also sensitive probes of more subtle local conformational changes in response to different 5′ sequences. Each ribozyme−substrate analogue complex shows distinct binding and dissociation kinetics (Figure 2 and Table 1), fluorescence intensity amplitudes (Figure 3), and emission lifetime distributions (Figure 5 and Table 2), consistent with the idea that each 5′ sequence leads to a distinct equilibrium of stacked versus unstacked AP_{76} conformations in the catalytic core. In all substrate complexes, AP_{76} is significantly more stacked than in complex with the 3′ product, in agreement with our previous results (*22*). Furthermore, the conformational changes in the catalytic core upon substrate analogue or 3′ product binding kinetically coincide for all complexes with the corresponding global conformational changes observed by steady-state FRET (Figure 6), consistent with the idea that both types of

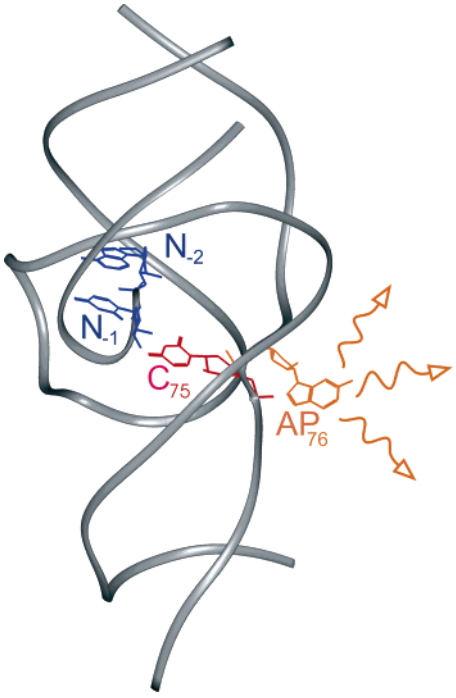

FIGURE 7: Effect of the N_{-1} and N_{-2} nucleotides of the 5′ sequence on the local stacking environment of AP_{76}, shown in the structural context of the cobalt-hexammine-containing crystal structure of the precursor form of the genomic HDV ribozyme (pdb ID 1SJF). AP_{76} (orange) is quenched in the free ribozyme and becomes partially unquenched (arrows) upon the addition of a noncleavable substrate analogue, depending in magnitude on its 5′ sequence. The identity of the N_{-1} and N_{-2} nucleotides, thus, affects the conformation of the HDV ribozyme's trefoil turn and, thereby, the stacking environment of AP_{76} and presumably that of the catalytic C_{75} (red) in the catalytic core at a distance of 16 Å between AP_{76} and N_{-1} and a distance of 18 Å between AP_{76} and N_{-2}. This Figure was prepared using Insight II (Accelrys Software Inc.).

structural dynamics are coupled. Consequently, the relative order of AP_{76} monitored binding rate constants (3′P > ncS1A > ncS1CC > ncS2C > ncS2UC > ncS1U> ncS3UUC; Table 1) is similar to that observed in previous FRET analyses in the absence of the AP_{76} probe (*34*). The longest substrate analogue, ncS3UUC, binds most slowly and induces the lowest AP_{76} fluorescence increase relative to the substrate-free ribozyme, possibly due to the competition of its 5′ sequence with the formation of the short ribozyme helix P1.1 (Figure 1). Notably, the binding of the shortest substrate analogue, the 3′ product, is fastest and induces the highest fluorescence increase without a significant 3′P concentration dependence. This observation suggests that the resulting conformational relaxation of the trefoil turn and not the 3′P binding is rate-limiting in this case. There is, however, no general correlation between the fluorescence increase amplitude and k_{on} of substrate analogue binding (compare Figure 2 and Table 1).

When comparing our results for local conformation in the catalytic core in response to different 5′ sequences with the corresponding data for cleavage activity (*9*, *34*), we find that a U in the N_{-1} position causes slow binding but fast cleavage. This indicates that reaction chemistry could, in fact, be rate-limiting for the cleavage of this substrate. A C in the N_{-1} position (as in ncS1C, ncS2CC, ncS2UC, and ncS3UUC) is found to lead from very slow binding (ncS3UUC, 1.4×10^4 min^{-1} M^{-1}) to 2 orders of magnitude faster binding (ncS2CC, 1.4×10^6 min^{-1} M^{-1}) as well as from very slow cleavage (S2CC, 0.01 min^{-1}) to relatively fast cleavage (S1C, 2.7 min^{-1}), depending on the identities of the nucleotides in the N_{-2} and N_{-3} positions, with no strong correlation between binding and cleavage rate constants, as discussed before (*34*).

Magnesium Aids Formation of the Trefoil Turn of the Catalytic Core. RNA generally shows a dependence on metal ions for folding and catalysis. The HDV ribozyme is no exception. Crystal structures (*19*−*21*), FRET analyses (*36*), terbium-footprinting (*43*), and, now, AP-fluorescence all corroborate the importance of metal ions, especially Mg^{2+}, for the folding of the HDV ribozyme. For example, the rate constant of 3′ product binding is clearly Mg^{2+}-dependent with a magnesium half-titration point of 2.6 mM, whereas a magnesium titration of the assembled ribozyme-3′ product complex shows an increase in the AP_{76} fluorescence signal chiefly below 3 mM Mg^{2+} (Figure 4). These observations imply that AP_{76} is not unstacked to its fullest extent until a slightly higher than physiologic (1−2 mM) Mg^{2+} concentration is reached. Interestingly, a refined crystal structure of the product form of the genomic HDV ribozyme has revealed a specific Mg^{2+} binding site next to G_{76} of the trefoil turn motif (*20*). Our data suggest that such Mg^{2+} binding aids the formation of the trefoil turn that extrudes the nucleotide in position 76.

Picosecond Time-Resolved AP_{76} Fluorescence Suggests that the Trefoil Turn in the Catalytic Core is in a Dynamic Equilibrium of Conformations, in Contrast to the Single Conformation Observed in the Crystal Structure. A comparison of the AP_{76} fluorescence decay curves reveals a significant difference between all ribozyme−noncleavable substrate analogue and product complexes (Figure 5), yet Table 2 demonstrates that each complex is best described by a conformational equilibrium that harbors (at least) four different conformations in which AP_{76} is fully unstacked (fastest decay component), fully stacked (slowest decay component), or partially stacked (two intermediate decay components) (*39*, *40*, *44*, *45*). X-ray crystallography of the cis-acting genomic HDV ribozyme shows a single conformation in which G_{76} is extruded into solvent, thereby pushing the catalytically involved C_{75} deeper into the catalytic core as part of the trefoil turn motif (*19*, *21*). However, there is likely a bias in the crystal structure toward the formation of this specific conformation because of crystal lattice contacts involving the stacking of two extruded G_{76} nucleotides from adjacent molecules (*20*). It is plausible to assume that once this stacking constraint is removed in solution the position of the nucleotide in position 76 is generally dynamic so that it samples different conformational states, as deduced from our AP_{76} decay data. Along this line of thinking, changes in catalytic core conformation upon introduction of different 5′ sequences (at a distance of 16−18 Å; Figure 7) or upon substrate cleavage simply lead to subtle adjustments in the equilibrium ensemble of trefoil turn conformations. Picosecond time-resolved AP spectroscopy, as shown in Figure 5 and analyzed in Table 2, provides snapshots of the variety of conformations around the spectroscopic probe, AP_{76}. Complementary steady-state AP fluorescence measurements amplify these conformational adjustments into significant signal changes that can be readily detected as demonstrated here.

One can correlate our observations with recent ns molecular dynamics simulations, which indicate that C_{75} in the pre-cleavage structure shows a rather weak and, therefore, dynamic binding in the catalytic core (*58*). The adjacent G_{76} moves freely and can turn within less than a ns by large torsional angles, which impacts the positioning of C_{75} within the catalytic core and presumably catalysis (unpublished data). Clearly, the trefoil turn (joiner J4/2) is one of the most dynamic regions of the HDV ribozyme, particularly prior to catalysis. In comparison, in the product form, C_{75} is more deeply lodged and more stably hydrogen bonded in the catalytic pocket (*58*). These computational analyses are qualitatively consistent with the experimental data reported here, which show that the fluorescence of AP_{76} is quenched by a larger sampling of stacked conformations in the pre-cleavage form compared to that in the product form, allowing the position of the adjacent C_{75} to fluctuate. AP_{76} fluorescence significantly increases upon cleavage and dissociation of the 5′ substrate sequence to form the product, indicating that the 76 position becomes unstacked or exposed to the solvent, consistent with the deeper anchoring of C_{75} within the catalytic core. This complementarity of experimental and computational results further supports the notion that the trefoil turn is in a dynamic equilibrium of conformations not depicted by the static crystal structures.

ACKNOWLEDGMENT

We thank Steve Katnick for help with setting up our laser-induced time-resolved spectrofluorometer and all members of the Walter lab for stimulating discussions.

REFERENCES

1. Gao, J. (2003) Catalysis by enzyme conformational change as illustrated by orotidine 5′-monophosphate decarboxylase, *Curr. Opin. Struct. Biol. 13*, 184−192.
2. Gutteridge, A., and Thornton, J. (2004) Conformational change in substrate binding, catalysis and product release: an open and shut case? *FEBS Lett. 567*, 67−73.
3. Schnell, J. R., Dyson, H. J., and Wright, P. E. (2004) Structure, dynamics, and catalytic function of dihydrofolate reductase, *Annu. Rev. Biophys. Biomol. Struct. 33*, 119−140.
4. Murray, J. B., Dunham, C. M., and Scott, W. G. (2002) A pH-dependent conformational change, rather than the chemical step, appears to be rate-limiting in the hammerhead ribozyme cleavage reaction, *J. Mol. Biol. 315*, 121−130.
5. Han, J., and Burke, J. M. (2005) Model for general acid-base catalysis by the hammerhead ribozyme: pH-activity relationships of G8 and G12 variants at the putative active site, *Biochemistry 44*, 7864−7870.
6. Walter, N. G., Hampel, K. J., Brown, K. M., and Burke, J. M. (1998) Tertiary structure formation in the hairpin ribozyme monitored by fluorescence resonance energy transfer, *EMBO J. 17*, 2378−2391.
7. Zhuang, X., Kim, H., Pereira, M. J., Babcock, H. P., Walter, N. G., and Chu, S. (2002) Correlating structural dynamics and function in single ribozyme molecules, *Science 296*, 1473−1476.
8. Rueda, D., Bokinsky, G., Rhodes, M. M., Rust, M. J., Zhuang, X., and Walter, N. G. (2004) Single-molecule enzymology of RNA: essential functional groups impact catalysis from a distance, *Proc. Natl. Acad. Sci. U.S.A. 101*, 10066−10071.
9. Shih, I., and Been, M. D. (2001) Energetic contribution of non-essential 5′ sequence to catalysis in a hepatitis delta virus ribozyme, *EMBO J. 20*, 4884−4891.
10. Shih, I. H., and Been, M. D. (2002) Catalytic strategies of the hepatitis delta virus ribozymes, *Annu. Rev. Biochem. 71*, 887−917.
11. Pereira, M. B., Harris, D. A., Rueda, D., and Walter, N. G. (2002) The reaction pathway of the trans-acting hepatitis delta virus ribozyme: a conformational change accompanies catalysis, *Biochemistry 41*, 730−740.
12. Lai, M. M. (1995) The molecular biology of hepatitis delta virus, *Annu. Rev. Biochem. 64*, 259−286.
13. Macnaughton, T. B., and Lai, M. M. (2002) Genomic but not antigenomic hepatitis delta virus RNA is preferentially exported from the nucleus immediately after synthesis and processing, *J. Virol. 76*, 3928−3935.
14. Kato, Y., Kuwabara, T., Warashina, M., Toda, H., and Taira, K. (2001) Relationships between the activities in vitro and in vivo of various kinds of ribozymes and their intracellular localization in mammalian cells, *J. Biol. Chem. 276*, 15378−15385.
15. Levesque, D., Choufani, S., and Perreault, J. P. (2002) Delta ribozyme benefits from a good stability in vitro that becomes outstanding in vivo. *RNA 8*, 464−477.
16. D'Anjou, F., Bergeron, L. J., Larbi, N. B., Fournier, I., Salzet, M., Perreault, J. P., and Day, R. (2004) Silencing of SPC2 expression using an engineered delta ribozyme in the mouse betaTC-3 endocrine cell line, *J. Biol. Chem. 279*, 14232−14239.
17. Bergeron, L. J., and Perreault, J. P. (2005) Target-dependent on/off switch increases ribozyme fidelity, *Nucleic Acids Res. 33*, 1240−1248.
18. Rosenstein, S. P., and Been, M. D. (1996) Hepatitis delta virus ribozymes fold to generate a solvent-inaccessible core with essential nucleotides near the cleavage site phosphate. *Biochemistry 35*, 11403−11413.
19. Ferre-D'Amare, A. R., Zhou, K., and Doudna, J. A. (1998) Crystal structure of a hepatitis delta virus ribozyme, *Nature 395*, 567−574.
20. Ferre-D'Amare, A. R., and Doudna, J. A. (2000) Crystallization and structure determination of a hepatitis delta virus ribozyme: use of the RNA-binding protein U1A as a crystallization module, *J. Mol. Biol. 295*, 541−556.
21. Ke, A., Zhou, K., Ding, F., Cate, J. H., and Doudna, J. A. (2004) A conformational switch controls hepatitis delta virus ribozyme catalysis, *Nature 429*, 201−205.
22. Harris, D. A., Rueda, D., and Walter, N. G. (2002) Local conformational changes in the catalytic core of the trans-acting hepatitis delta virus ribozyme accompany catalysis, *Biochemistry 41*, 12051−12061.
23. Tanaka, Y., Tagaya, M., Hori, T., Sakamoto, T., Kurihara, Y., Katahira, M., and Uesugi, S. (2002) Cleavage reaction of HDV ribozymes in the presence of Mg2+ is accompanied by a conformational change, *Genes Cells 7*, 567−579.
24. Luptak, A., Ferre-D'Amare, A. R., Zhou, K., Zilm, K. W., and Doudna, J. A. (2001) Direct p*K*(a) measurement of the active-site cytosine in a genomic hepatitis delta virus ribozyme, *J. Am. Chem. Soc. 123*, 8447−8452.
25. Been, M. D., and Wickham, G. S. (1997) Self-cleaving ribozymes of hepatitis delta virus RNA, *Eur J. Biochem. 247*, 741−753.
26. Ward, D. C., Reich, E., and Stryer, L. (1969) Fluorescence studies of nucleotides and polynucleotides. I. Formycin, 2-aminopurine riboside, 2,6-diaminopurine riboside, and their derivatives, *J. Biol. Chem. 244*, 1228−1237.
27. Doudna, J. A., Szostak, J. W., Rich, A., and Usman, N. (1990) Chemical synthesis of oligoribonucleotides containing 2-aminopurine: substrates for the investigation of ribozyme function, *J. Org. Chem. 55*, 5547−5549.
28. Fujimoto, J., Nuesca, Z., Mazurek, M., and Sowers, L. C. (1996) Synthesis and hydrolysis of oligodeoxyribonucleotides containing 2-aminopurine, *Nucleic Acids Res. 24*, 754−759.
29. Millar, D. P. (1996) Fluorescence studies of DNA and RNA structure and dynamics, *Curr. Opin. Struct. Biol. 6*, 322−326.
30. Rist, M. J., and Marino, J. P. (2002) Fluorescent nucleotide base analogs as probes of nucleic acid structure, dynamics and interactions. *Curr. Org. Chem. 6*, 775−793.
31. Nishikawa, F., and Nishikawa, S. (2000) Requirement for canonical base pairing in the short pseudoknot structure of genomic hepatitis delta virus ribozyme, *Nucleic Acids Res. 28*, 925−931.
32. Wadkins, T. S., Perrotta, A. T., Ferre-D'Amare, A. R., Doudna, J. A., and Been, M. D. (1999) A nested double pseudoknot is required for self-cleavage activity of both the genomic and antigenomic hepatitis delta virus ribozymes, *RNA 5*, 720−727.
33. Deschenes, P., Lafontaine, D. A., Charland, S., and Perreault, J. P. (2000) Nucleotides −1 to −4 of hepatitis delta ribozyme substrate increase the specificity of ribozyme cleavage. *Antisense Nucleic Acid Drug Dev. 10*, 53−61.
34. Jeong, S., Sefcikova, J., Tinsley, R. A., Rueda, D., and Walter, N. G. (2003) Trans-acting hepatitis delta virus ribozyme: catalytic

core and global structure are dependent on the 5′ substrate sequence, *Biochemistry 42*, 7727−7740.
35. Tinsley, R. A., Harris, D. A., and Walter, N. G. (2003) Significant kinetic solvent isotope effects in folding of the catalytic RNA from the hepatitis delta virus, *J. Am. Chem. Soc. 125*, 13972−13973.
36. Tinsley, R. A., Harris, D. A., and Walter, N. G. (2004) Magnesium dependence of the amplified conformational switch in the trans-acting hepatitis delta virus ribozyme, *Biochemistry 43*, 8935−8945.
37. Walter, N. G. (2001) Structural dynamics of catalytic RNA highlighted by fluorescence resonance energy transfer, *Methods 25*, 19−30.
38. Walter, N. G. (2002) Probing RNA structural dynamics and function by fluorescence resonance energy transfer (FRET), *Curr. Protocols Nucleic Acid Chem. 11.10*, 11.10.11−11.10.23.
39. Guest, C. R., Hochstrasser, R. A., Dupuy, C. G., Allen, D. J., Benkovic, S. J., and Millar, D. P. (1991) Interaction of DNA with the Klenow fragment of DNA polymerase I studied by time-resolved fluorescence spectroscopy, *Biochemistry 30*, 8759−8770.
40. Walter, N. G., Chan, P. A., Hampel, K. J., Millar, D. P., and Burke, J. M. (2001) A base change in the catalytic core of the hairpin ribozyme perturbs function but not domain docking, *Biochemistry 40*, 2580−2587.
41. Rachofsky, E. L., Osman, R., and Ross, J. B. (2001) Probing structure and dynamics of DNA with 2-aminopurine: effects of local environment on fluorescence, *Biochemistry 40*, 946−956.
42. Jean, J. M., and Hall, K. B. (2001) 2-Aminopurine fluorescence quenching and lifetimes: role of base stacking, *Proc. Natl. Acad. Sci. U.S.A. 98*, 37−41.
43. Harris, D. A., Tinsley, R. A., and Walter, N. G. (2004) Terbium-mediated footprinting probes a catalytic conformational switch in the antigenomic hepatitis delta virus ribozyme, *J. Mol. Biol. 341*, 389−403.
44. Hochstrasser, R. A., Carver, T. E., Sowers, L. C., and Millar, D. P. (1994) Melting of a DNA helix terminus within the active site of a DNA polymerase, *Biochemistry 33*, 11971−11979.
45. Rai, P., Cole, T. D., Thompson, E., Millar, D. P., and Linn, S. (2003) Steady-state and time-resolved fluorescence studies indicate an unusual conformation of 2-aminopurine within ATAT and TATA duplex DNA sequences, *Nucleic Acids Res. 31*, 2323−2332.
46. Wadkins, T. S., Shih, I., Perrotta, A. T., and Been, M. D. (2001) A pH-sensitive RNA tertiary interaction affects self-cleavage activity of the HDV ribozymes in the absence of added divalent metal ion, *J. Mol. Biol. 305*, 1045−1055.
47. Walter, N. G., and Engelke, D. R. (2002) Ribozymes: catalytic RNAs that cut things, make things, and do odd and useful jobs, *Biologist (London) 49*, 199−203.
48. Zamore, P. D., and Haley, B. (2005) Ribo-gnome: the big world of small RNAs, *Science 309*, 1519−1524.
49. Carninci, P., Kasukawa, T., Katayama, S., Gough, J., Frith, M. C., Maeda, N., Oyama, R., Ravasi, T., Lenhard, B., Wells, C., Kodzius, R., Shimokawa, K., Bajic, V. B., Brenner, S. E., Batalov, S., Forrest, A. R., Zavolan, M., Davis, M. J., Wilming, L. G., Aidinis, V., Allen, J. E., Ambesi-Impiombato, A., Apweiler, R., Aturaliya, R. N., Bailey, T. L., Bansal, M., Baxter, L., Beisel, K. W., Bersano, T., Bono, H., Chalk, A. M., Chiu, K. P., Choudhary, V., Christoffels, A., Clutterbuck, D. R., Crowe, M. L., Dalla, E., Dalrymple, B. P., de Bono, B., Della Gatta, G., di Bernardo, D., Down, T., Engstrom, P., Fagiolini, M., Faulkner, G., Fletcher, C. F., Fukushima, T., Furuno, M., Futaki, S., Gariboldi, M., Georgii-Hemming, P., Gingeras, T. R., Gojobori, T., Green, R. E., Gustincich, S., Harbers, M., Hayashi, Y., Hensch, T. K., Hirokawa, N., Hill, D., Huminiecki, L., Iacono, M., Ikeo, K., Iwama, A., Ishikawa, T., Jakt, M., Kanapin, A., Katoh, M., Kawasawa, Y., Kelso, J., Kitamura, H., Kitano, H., Kollias, G., Krishnan, S. P., Kruger, A., Kummerfeld, S. K., Kurochkin, I. V., Lareau, L. F., Lazarevic, D., Lipovich, L., Liu, J., Liuni, S., McWilliam, S., Madan Babu, M., Madera, M., Marchionni, L., Matsuda, H., Matsuzawa, S., Miki, H., Mignone, F., Miyake, S., Morris, K., Mottagui-Tabar, S., Mulder, N., Nakano, N., Nakauchi, H., Ng, P., Nilsson, R., Nishiguchi, S., Nishikawa, S., et al. (2005) The transcriptional landscape of the mammalian genome, *Science 309*, 1559−1563.
50. Menger, M., Tuschl, T., Eckstein, F., and Porschke, D. (1996) Mg(2+)-dependent conformational changes in the hammerhead ribozyme, *Biochemistry 35*, 14710−14716.
51. Menger, M., Eckstein, F., and Porschke, D. (2000) Multiple conformational states of the hammerhead ribozyme, broad time range of relaxation and topology of dynamics, *Nucleic Acids Res. 28*, 4428−4434.
52. Pinard, R., Hampel, K. J., Heckman, J. E., Lambert, D., Chan, P. A., Major, F., and Burke, J. M. (2001) Functional involvement of G8 in the hairpin ribozyme cleavage mechanism, *EMBO J. 20*, 6434−6442.
53. Parrott, A. M., Lago, H., Adams, C. J., Ashcroft, A. E., Stonehouse, N. J., and Stockley, P. G. (2000) RNA aptamers for the MS2 bacteriophage coat protein and the wild-type RNA operator have similar solution behaviour, *Nucleic Acids Res. 28*, 489−497.
54. Jucker, F. M., Phillips, R. M., McCallum, S. A., and Pardi, A. (2003) Role of a heterogeneous free state in the formation of a specific RNA-theophylline complex, *Biochemistry 42*, 2560−2567.
55. Rist, M., and Marino, J. (2001) Association of an RNA kissing complex analyzed using 2-aminopurine fluorescence, *Nucleic Acids Res. 29*, 2401−2408.
56. Menger, M., Eckstein, F., and Porschke, D. (2000) Dynamics of the RNA hairpin GNRA tetraloop, *Biochemistry 39*, 4500−4507.
57. Lacourciere, K. A., Stivers, J. T., and Marino, J. P. (2000) Mechanism of neomycin and Rev peptide binding to the Rev responsive element of HIV-1 as determined by fluorescence and NMR spectroscopy, *Biochemistry 39*, 5630−5641.
58. Krasovska, M. V., Sefcikova, J., Spackova, N., Sponer, J., and Walter, N. G. (2005) Structural dynamics of precursor and product of the RNA enzyme from the hepatitis delta virus as revealed by molecular dynamics simulations, *J. Mol. Biol. 351*, 731−748.

BI052116J